Lawrence Berkeley National Laboratory
LBL Publications

Title
Geothermal Play Fairway Analysis, Part 2: GIS methodology

Permalink
https://escholarship.org/uc/item/7c80h8jm

Authors
DeAngelo, Jacob
Shervais, John W
Glen, Jonathan M
et al.

Publication Date
2024-02-01

DOI
10.1016/j.geothermics.2023.102882

Copyright Information
This work is made available under the terms of a Creative Commons Attribution License, available at https://creativecommons.org/licenses/by/4.0/

Peer reviewed

eScholarship.org Powered by the California Digital Library
University of California

Geothermics 117 (2024) 102882

Contents lists available at ScienceDirect

Geothermics

journal homepage: www.elsevier.com/locate/geothermics

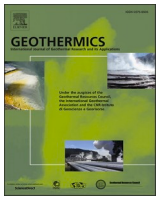

Geothermal Play Fairway Analysis, Part 2: GIS methodology

Jacob DeAngelo [a,*], John W. Shervais [b], Jonathan M. Glen [a], Dennis Nielson [c], Sabodh Garg [d], Patrick F. Dobson [e], Erika Gasperikova [e], Eric Sonnenthal [e], Lee M. Liberty [f], Drew L. Siler [a,d], James P. Evans [b]

[a] U.S. Geological Survey, 350 N. Akron Rd. P.O. Box 158 Moffett Field, CA 94035, United States
[b] Utah State University, Logan, UT, United States
[c] DOSECC Exploration Services, Salt Lake City, UT, United States
[d] Geologica Geothermal Group, Inc, 9920 Pacific Heights Blvd, Suite 150, San Diego, CA 92121, United States
[e] Lawrence Berkeley National Laboratory, Berkeley, CA, United States
[f] Boise State University, Boise, ID, United States

ARTICLE INFO

Keywords:
Geothermal Play Fairway Analysis
Snake River Plain
Resource favorability
Geothermal exploration
GIS
Python

ABSTRACT

Play Fairway Analysis (PFA) in geothermal exploration originates from a systematic methodology developed within the petroleum industry and is based on a geologic, geophysical, and hydrologic framework of identified geothermal systems. We tailored this methodology to study the geothermal resource potential of the Snake River Plain and surrounding region, but it can be adapted to other geothermal resource settings. We adapted the PFA approach to geothermal resource exploration by cataloging the critical elements controlling exploitable hydrothermal systems, establishing risk matrices that evaluate these elements in terms of both probability of success and level of knowledge, and building a code-based 'processing model' to process results.

A geographic information system was used to compile a range of different data types, which we refer to as elements (*e.g.*, faults, vents, heat flow, etc.), with distinct characteristics and measures of confidence. Discontinuous discrete data (points, lines, or polygons) for each element were transformed into continuous interpretive 2D grid surfaces called evidence layers. Because different data types have varying uncertainties, most evidence layers have an accompanying confidence layer which reflects spatial variations in these uncertainties. Risk layers, as defined here, are the product of evidence and confidence layers, and are the building blocks used to construct Common Risk Segment (CRS) maps for heat, permeability, and seal, using a weighted sum for permeability and heat, but a different approach with seal. CRS maps quantify the variable risk associated with each of these critical components. In a final step, the three CRS maps were combined into a Composite Common Risk Segment (CCRS) map, using a modified weighted sum, for results that reveal favorable areas for geothermal exploration. Additional maps are also presented that do not mix contributions from evidence and confidence (to allow an isolated view of evidence and confidence), as well as maps that calculate favorability using the product of components instead of a weighted sum (to highlight where all components are present). Our approach helped to identify areas of high geothermal favorability in the western and central Snake River Plain during the first phase of study and helped identify more precise local drilling targets during the second phase of work. By identifying favorable areas, this methodology can help to reduce uncertainty in geothermal energy exploration and development.

1. Introduction

The work described herein was undertaken as part of an effort to assess undiscovered geothermal resources across the Snake River Plain (SRP) of southern Idaho and surrounding regions (Fig. 1). The project scope and findings are presented in a companion paper (Shervais et al., 2024), and this paper is devoted to describing the methodology. Terminology specific to this study are italicized in their first usage and are contained in a glossary.

Play Fairway Analysis (PFA) evaluates the favorability of resource

* Corresponding author.
E-mail address: jdeangelo@usgs.gov (J. DeAngelo).

https://doi.org/10.1016/j.geothermics.2023.102882
Received 28 March 2023; Received in revised form 13 November 2023; Accepted 17 November 2023
Available online 4 December 2023
0375-6505/Published by Elsevier Ltd. This is an open access article under the CC BY-NC-ND license (http://creativecommons.org/licenses/by-nc-nd/4.0/).

occurrence within a specified area by identifying the general factors, or *components* responsible for their occurrence. The three components examined in this study are: *permeability, heat source*, and *seal*. Each component consists of a group of *elements* (*e.g.,* faults, vents, heat flow, etc.) that contribute to that component. *Common Risk Segment (CRS)* maps for each component were created by combining data from all the elements contributing to that component. For example, the CRS map for permeability was created by combining data representing mapped faults and structures inferred from geophysics. The CRS map for heat source was created by combining data representing regional heat flow, vents, helium isotope ratios, calculated multicomponent equilibrium reservoir temperatures, and measured groundwater temperatures. The CRS map for seal was made by combining data representing the extent of impermeable lake sediments and regional aquifers with a hydrothermally altered clay seal. CRS maps from these three components were used to produce the final predictive surface, the *Composite Common Risk Segment (CCRS)* map.

2. Approach

Our geographic information system (GIS) approach is similar to that used by earlier investigations that pioneered the use of GIS in geothermal exploration (*e.g.,* Coolbaugh et al. 2002, 2005, Noorollahi et al. 2008, Trumpy et al. 2015), and was developed in parallel with recent DOE-funded PFA projects in the United States (*e.g.,* Lautze et al. 2017a, 2017b, Ito et al. 2017). Raw data were first converted into ArcGIS shapefiles that used a common projection (Esri, 2023). These data files were used as inputs in a custom Python-based 'processing model' that automated most data-processing tasks associated with the production of CRS, CCRS, and other maps (Van Rossum and Drake, 1995).

Our study used a *knowledge-driven (or expert-driven)* approach in establishing weights and confidence values. Knowledge-driven approaches estimate weight values based on expert opinion whereas *data-driven* approaches establish weights by use of statistical relationships between elements and known occurrences of the phenomenon being modeled (Bonham-Carter, 1994). We employed a knowledge-driven approach because there were too few geothermal systems in the study area to draw meaningful results about the strength of the relationship between any given element and the presence of geothermal systems (*i.e.*, not enough training data). A data-driven approach requires the ability to compare elements to known occurrences of the phenomenon being predicted (training data). At present, there is only one operating geothermal plant in Idaho (Raft River) on the margins of the SRP in a Basin and Range type setting that may not be characteristic of many of the systems in the SRP.

The SRP is divided into three distinct regions. The Central (CSRP) and Eastern SRP (ESRP) lie on the Yellowstone-Snake River Plain plume track but are largely underlain by an enormous cold-water aquifer (the Snake River aquifer; Lindholm, 1996), which suppresses surface heat flux (McLing et al., 2016; Lachmar et al., 2017). In contrast, the western SRP (WSRP) is overlain by lake sediments that prevent hydrothermal fluids from rising to the surface (Lachmar et al., 2019). As a result, most potential geothermal systems beneath the SRP would be blind (no obvious surface expression), thus requiring unconventional methods for characterization of resource potential. Our strategy to undertake a preliminary assessment to identify these blind systems relied on assigning relative weight values in a weighted sum model to the elements and components based on the judgement of geoscientists familiar with the local controls on geothermal systems.

2.1. Terminology

We developed a uniform terminology for discussing GIS layers that are used and produced in the processing model. These layers are: (1) *data layers*, (2) *evidence layers*, (3) *confidence layers*, (4) *risk layers*, (5) CRS maps, (6) the CCRS map, (7) *evidence only* or *confidence only* maps, and (8) *product* maps.

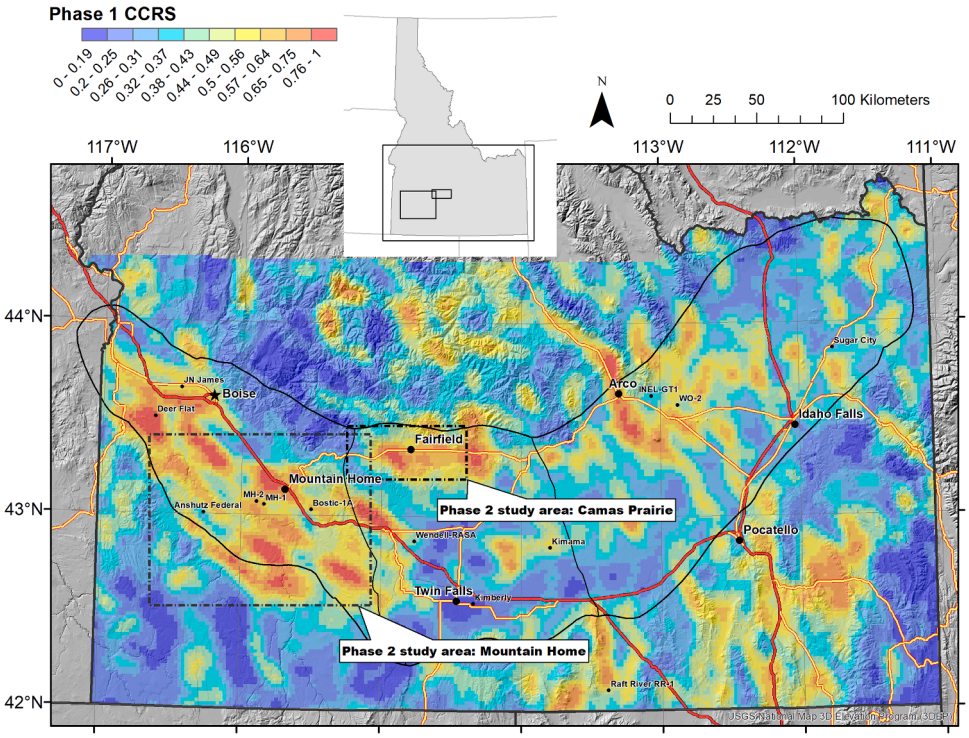

Fig. 1. Phase 1 Composite Common Risk Segment (CCRS) map, showing geothermal favorability predictions within the Phase 1 study area; warmer colors indicate higher favorability. Subregions (Western, Central, and Eastern SRP) are outlined with solid black lines. Red and yellow lines represent roads. Locations of Phase 2 study areas are shown with dotted outlines. Hillshade from USGS 3D Elevation Program (U.S. Geological Survey, 2019).

(1) Data layers are the original data that are used as inputs for data processing. These data use a common projection and may include points, lines, or polygons, many of which include important attribute information. In some cases, raw data were pre-processed before being transformed into evidence layers; for example, fault and lineament segments were evaluated for slip and dilation tendency prior to geoprocessing into evidence layers (*e.g.,* Morris et al. 1996).
(2) Evidence layers are created by applying geoprocessing tools to data layers. Tools used include the application of either a *density function* (simple or kernel density), which calculates the occurrence of objects within a given area, or a data *interpolation* function, which calculates intermediate values from a finite array of data points. Surfaces generated using these processes reflect the magnitude of the phenomena being modeled in their native units, for example the estimated heat flow or the density of volcanic vents in every cell of the study area. Surfaces in native units become evidence layers after being scaled to values ranging from 0 to 1.
(3) Confidence layers reflect uncertainties in evidence layers and range from 0 to 1, with zero reflecting no confidence and 1 reflecting complete confidence. These user-assigned values are assigned to map layers representing measured uncertainty. Interpolated evidence layers, for example, use the accompanying kriging standard error surface. Confidence for gravity is based on the distance to the nearest gravity measurement station. Confidence for mapped faults is based on published map scale (higher certainty for 1:24,000 scale, lower certainty for 1:250,000 scale). Confidence for magnetics is based on the survey quality (Drenth and Grauch, 2019).
(4) Risk layers are the result of applying the confidence layer to the evidence layer. Risk layers are produced by multiplying the evidence layer (which shows likelihood of a resource characteristic being present) with the appropriate confidence layer (which assesses likelihood of data being reliable or complete).
(5) CRS maps for the permeability and heat source components are the weighted sum of the risk layers within each component. Because each of these CRS maps represents the combination of multiple risk layers, and not all layers are equally diagnostic, a weighted sum is used to emphasize those layers that are thought to contribute most strongly to the characteristic in question, or to balance layers with different data densities that may contribute equally to that characteristic. The Seal CRS map was not constructed as a weighted sum.
(6) The CCRS map is the weighted sum of the permeability and heat source CRS maps multiplied by the Seal CRS map, then scaled from 0 to 1. This is the map that was used to assess resource favorability.
(7) Evidence only and confidence only maps for the permeability and heat source components are the weighted sum of the evidence layers and confidence layers respectively within each component. These maps allow for just the evidence or just the confidence of a component to be examined without combining their influences as in the CRS map. Combining these component-scale maps results in CCRS-scale evidence only and confidence only maps.
(8) Product maps were generated for CCRS, and the CRS-scale evidence only and confidence only maps. Instead of using a weighted sum, the product maps take the quotient of values from the three components. This approach is intended to favor places that have high estimated favorability in all components, not just some.

2.2. Processing workflow

The main GIS workflow of the study was carried out using tools built in Python, a scripting language that can execute geoprocessing tools in ArcMap and perform custom data manipulation and organization. These Python-based tools automate data processing to enhance the flexibility of the data analysis making it easily adaptable to perform assessments in other settings.

2.2.1. Data transformation types

Processing data layers into evidence layers typically involved either density functions to calculate the density distribution of an attribute or interpolation to calculate a continuous surface from point data (*e.g.*, heat flow or groundwater temperatures). Density functions are used for data that are discontinuous by nature and where the geographic location of that data is important. Interpolation is used for data that are by nature continuous but are only sampled at points.

Simple density functions count the number of like objects within a given radius (*e.g.*, 10 km for faults in Phase 1) and calculate the density by dividing the sum by the area of the search radius. The calculated density is assigned to the entire radius. Kernel density functions assess data density by counting all instances of the data within a specified radius of a single point and dividing by the area of the search radius. This density is then distributed from a maximum at the location of the data to zero at the full radius of the search area using a quadratic function. Data may be weighted prior to counting. For example, fault segments and structural lineations are weighted by both dilation tendency and slip tendency on a scale from zero to 1.0, as a measure of their likelihood to serve as permeable pathways for fluid flow (Morris et al., 1996; Ferrill et al., 1999; see also Shervais et al., 2024).

For interpolated layers, we used *Empirical Bayesian Kriging* (*EBK*), a geostatistical process that produces an estimate of the value of a property at each point on a continuous surface and a standard error surface that quantifies the uncertainty in the interpolation (Krivoruchko and Gribov, 2020). Standard kriging methods use existing data locations to predict the values at unknown locations. With EBK, a variogram is calculated using the original data. This variogram is then used to create a simulated dataset using an intrinsic random function and a variogram of the simulated data is created. Bayes' rule is used to determine how likely the original data could be created by the variogram of the simulated data and weights it accordingly (Bayes, 1764). Prediction and prediction errors are derived using these weights. As a result, EBK claims to return a more generalized interpolation and a more robust estimate of standard errors compared to other kriging methods (Esri, 2023).

2.2.2. Confidence

Confidence levels are assigned using a fuzzy logic approach (user defined limits that range from 0 to 1). For interpolated surfaces using EBK the values are chosen based on the standard error map, with highest confidence (1.0) at the lowest standard errors and progressively lower confidence (values less than 1.0) at higher standard errors. Confidence values can be set to zero in places with no confidence, (as with the RTEst multicomponent geothermometer estimates (Neupane et al., 2014) that exceeded reasonable uncertainties), but confidence values generally ranged from a maximum of 1.0 to minimums at or above 0.5. For faults, the scale of mapping and map publication are important because regional scale mapping may simplify or omit some faults. This is particularly important to capture with a confidence layer because faults and structural complexity are considered important factors controlling geothermal systems (Faulds and Hinz, 2015). Local scale maps (1:24,000) were assigned higher confidence scores than regional scale maps (1:250,000). Similarly, the confidence layer for magnetic data is based on the coverage density of the sampled data used to generate structural lineations. The confidence layer for gravity data, however, is based on the distance from the nearest gravity station measurement.

2.2.3. GIS processing model

The GIS processing model, along with all data inputs and outputs, required tables, and documentation are available in data releases associated with Phase 1 and Phase 2 of this project (DeAngelo et al., 2021a, 2021b). The processing model performs a series of steps defined in a set

of input tables. A 'parameter table' includes the name of GIS files for evidence and confidence data as well as instructions on how to use those data. For example, if an element uses a pre-existing grid (like an interpolated surface), those surfaces must be directly sampled. If a density function is used on a data layer, such as lines or points (faults or vents), the user can specify a kernel or simple density, a weighting attribute, and a search radius. There are options to sample weights associated with categories from polygon inputs (*e.g.*, aquifer or lacustrine extent), and to assign weights based on the distance to a feature, which can accommodate specifying weights to specific distance intervals. Similarly, for confidence data, options exist to directly sample a preexisting surface, to use weights associated with categories from polygon inputs, or to assign weights based on the distance from a feature. Different options exist for data scaling, and there are custom options to accommodate processing choices made for this study.

A coefficient table stores static coefficients chosen by expert opinion, for example: the relative weights of elements within a component, relative weights between components, confidence weights applied to confidence layers, scaling parameters, evidence weights, and distance thresholds. Each list of coefficients has a unique name that is used by the parameter table to access coefficient lists. A study area raster is chosen by a user to define the projection, processing extent, and cell size of the study. A user must also specify the name of a master points file that will contain all sampled and calculated data. The processing model generates output layers corresponding to evidence layers, confidence layers, CRS, CCRS, evidence only and confidence, and product maps.

3. Data and results

The three geothermal play components examined in this study (permeability, heat source, and seal) are defined by distinct elements (or geologic phenomena) which require different approaches to generate evidence layers and confidence layers, and to compute CRS maps. In this section we describe each element within each component in the Phase 1 data. Section 4 describes changes made in Phase 2. All Phase 1 grids cover the same extent using a 2 km spacing (Fig. 1).

3.1. Permeability

Four elements were examined in constructing the permeability CRS map: (1) mapped faults; and lineations interpreted from maximum horizontal gradients of (2) mid-depth gravity anomalies, (3) deep gravity anomalies, and (4) magnetic field (pseudogravity) anomalies. These geophysically defined lineations reflect major lateral contrasts in density and magnetic properties that reveal potential structural features (*e.g.*, faults or contacts) in the subsurface. These features can provide pathways for fluid flow (*e.g.*, Shervais et al. 2014). The structures inferred from the gravity and magnetics data provide insights into potential buried permeable structures that would not be possible to detect in much of the SRP province if only mapped faults were considered (Fig. 2), given that much of the area is covered by Pliocene-Pleistocene volcanic flows and lacustrine deposits that obscure older structures. Mapped fault data are from the U.S. Geological Survey (USGS) Quaternary fault database (Machette et al., 2003) and Idaho Geological Survey (Ludington et al., 2005). Geophysical data for the Phase 1 region were compiled from a variety of sources (Bankey et al., 2002; McCafferty et al., 1999; Hildenbrand et al., 2002).

Faulds and Hinz (2015) have shown that geothermal permeability is favored by specific types of structural settings such as fault intersections, step-overs, and accomodation zones. Identifying these features from large or intermediate scale regional mapping is not practical, however, we chose an alternate approach that uses the density of faults and lineaments as a proxy for fault intersections. Thus, it is expected that areas with high densities of faults or lineaments are more likely to have fault intersections and fault-generated permeability. Once smaller scale prospects have been identified, fault density could be replaced or supplemented by mapped fault intersections as proposed by Faulds and Hinz (2015).

For each element, two kernel density surfaces were created with a 10 km search radius: one weighted by dilation tendency and the other by slip tendency (Siler et al., 2016; Shervais et al., 2024) (Fig. 2). To scale the evidence layers from the four different elements in a way that made them directly comparable to one another, each was scaled using the same maximum and minimum (zero) values. The maximum value was taken from the highest of the four evidence layer maximums. For example, the data layer for mapped faults (Fig. 2) contains many more

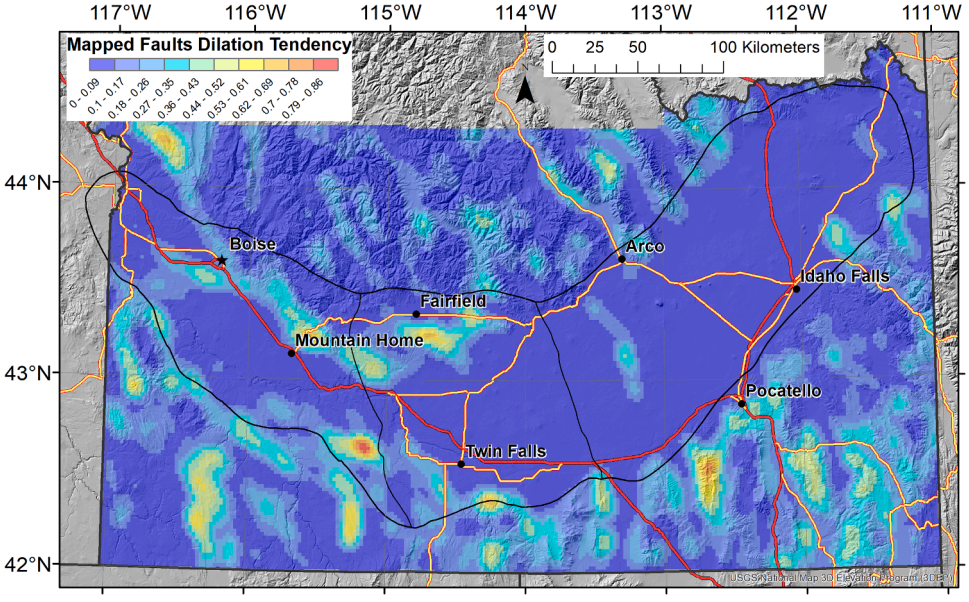

Fig. 2. Kernel density surface of mapped faults weighted by dilation tendency. Surface values with warmer colors indicate greater dilation tendency (increased permeability). Similar surfaces were created for magnetic, mid-depth gravity, and deep gravity lineations for both dilation tendency and slip tendency. Red and yellow lines represent roads. Hillshade from USGS 3D Elevation Program (U.S. Geological Survey, 2019).

line segments per unit area than the data layer for any of the other three elements examined for permeability. The mapped faults evidence layer therefore had a higher maximum density than the evidence layers from the other elements and in our case, the maximum density value from mapped faults was used to scale. This was done separately for the dilation tendency and slip tendency evidence layers. By using the largest maximum value instead of each layer's maximum, density values between different data types all reflect the same features per unit area. These scaled values were later combined with values from the confidence layers to calculate risk layers for permeability.

Confidence layers for mapped faults and magnetics were derived from polygon files that show the scale of sampling across the study area. Before being used in the processing model, polygons in each file were manually assigned codes indicating highest to lowest confidence. These codes correspond to user-defined weights or confidence values (Fig. 3-A, B). The two elements derived from gravity both used the same confidence layer and weights. The confidence layer for both gravity elements was constructed in the processing model by assigning weights based on distance to the nearest gravity station (Fig. 3-C). First, a surface was created from the gravity station point locations showing the distance to the nearest gravity station. This distance-surface was transformed using a list of distances and a list of weights (user-defined) to assign those weights for each distance bin.

The risk values for each element were calculated by multiplying the scaled evidence and confidence values. The CRS value for permeability was calculated by multiplying each risk element by its weight from the list of weights for permeability, summing those products together, and scaling the data (Fig. 4).

3.2. Heat source

Five elements were examined in constructing the heat source CRS map: volcanic vents (locations, ages, and density), heat flow, helium isotopic composition in hot springs and wells, multicomponent geothermometry equilibrium reservoir temperatures in hot springs and wells, and groundwater temperatures.

Volcanic vents were represented as point locations (Shervais et al., 2015, 2016, 2024). Before processing, vents were assigned codes describing their size and age in order of relevance. These size and age codes corresponded to lists of weights for size and age. For each vent, the weight value from its age category was multiplied by the weight value from its size category and stored as the vent's overall weight. This weight value was used in a weighted kernel density surface (10 km search radius) and scaled to create the evidence layer (Fig. 5). No confidence layer was used with vents, the scaled evidence layer therefore serves as the risk layer for vents.

Helium isotope data were represented as point locations of analyzed spring and well water samples using measured $^{3}He/^{4}He$ ratios relative to air (R/Ra) (Dobson et al., 2015). Those values were used to weight a simple density function and create a density surface (10 km radius). A simple density function was used in this case because samples were believed to reflect the local conditions. No confidence data were used, and scaled values were used as the evidence layer and risk layer for helium.

Heat flow data were compiled from USGS and Southern Methodist University Geothermal Lab databases *(e.g.,* Blackwell, 1989; Blackwell and Richards, 2004; Williams and DeAngelo, 2008, 2011). These data were represented as point data. To reduce the effects of very high measurements on the regional heat flow estimates and better represent background conductive conditions, wells with heat flow over 120

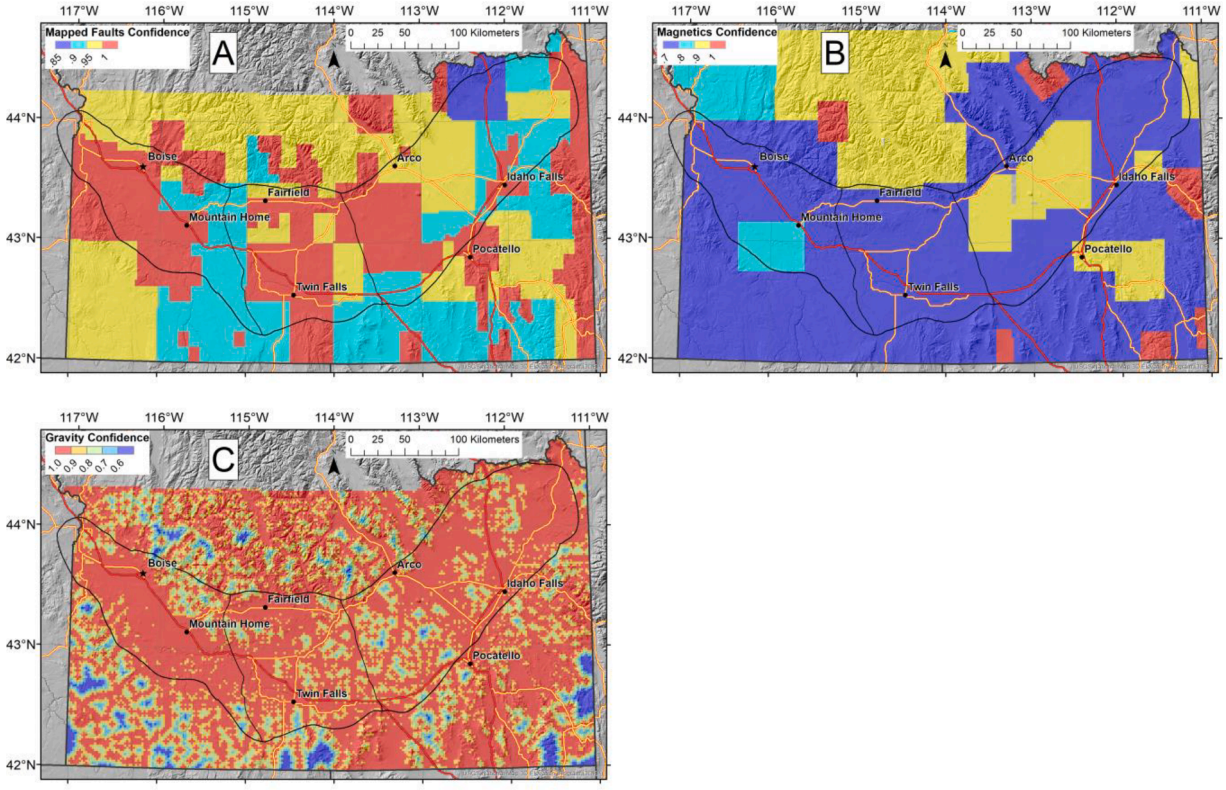

Fig. 3. Confidence maps for permeability elements. Each shows the confidence value applied across the study area. (A) Confidence for mapped faults determined by the scale of geologic mapping in the area showing level of uncertainty in original measurements. (B) Confidence for magnetics determined by the flight specifications of aeromagnetic surveys showing level of uncertainty characterized by line spacing and elevation above terrain. (C) Confidence for gravity showing level of uncertainty defined by distance to nearest gravity station. Hillshade from USGS 3D Elevation Program (U.S. Geological Survey, 2019).

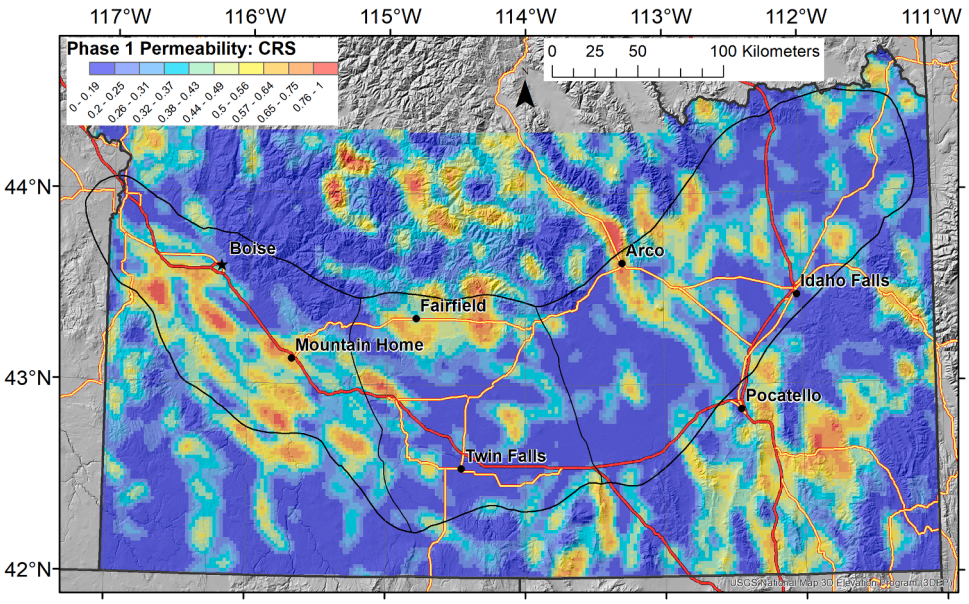

Fig. 4. Common risk segment (CRS) map for Permeability: eight risk layers (four elements, each weighted by dilation and slip tendency) were weighted and combined to create the CRS map. Warm colors indicate regions with high favorability. Red and yellow lines represent roads. Hillshade from USGS 3D Elevation Program (U.S. Geological Survey, 2019).

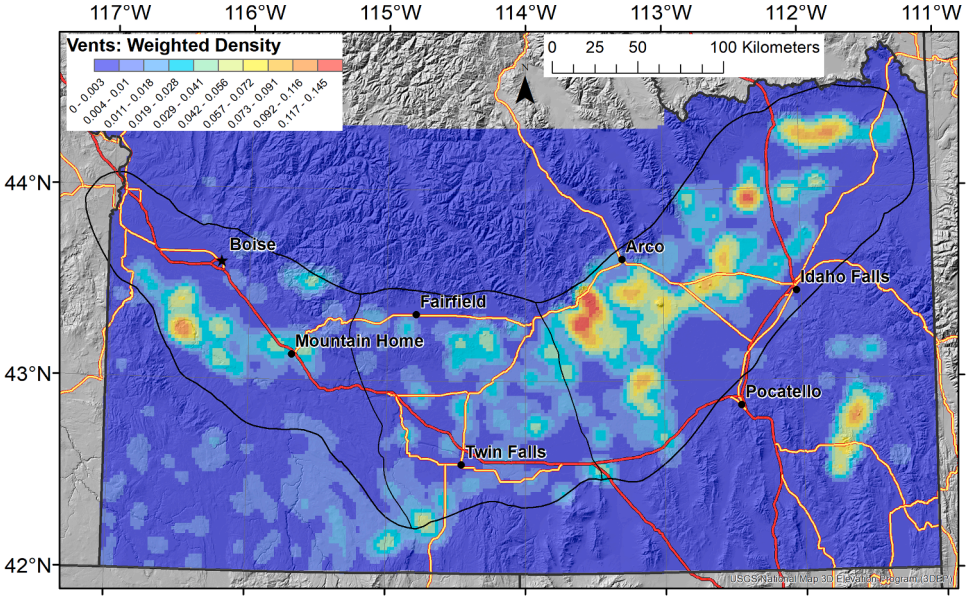

Fig. 5. Kernel density surface of vents weighted by age and size. The product of the weights for age and size were used to weight the surface. Red and yellow lines represent roads. Hillshade from USGS 3D Elevation Program (U.S. Geological Survey, 2019).

mW/m^2 were set to equal 120 mW/m^2. Additionally, wells that appeared to depict thermal conductivity in a cold regional aquifer were removed. The data were interpolated using EBK into a surface estimating heat flow across the region (Fig. 6A). A surface estimating the standard error of the heat flow prediction was also created (Fig. 6B). These surfaces were used as inputs in the processing model. The heat flow prediction values were then scaled using a user-defined minimum and maximum value. These scaled values were later combined with values from the confidence layer to calculate the risk layer for heat flow. The confidence layer was created by breaking up the standard error surface into five bins with each bin representing an equal portion of the standard error values between the minimum and maximum values. These bins were assigned a confidence value from a user-specified list.

Multicomponent geothermometer reservoir temperatures (Neupane et al., 2014; Cannon et al., 2014), were interpolated using EBK for prediction and standard error by the same means as the heat flow data before being used as an input for the processing model. Confidence values were assigned based on the standard error surface using the same process as heat flow data. The approach taken with multicomponent equilibrium reservoir temperatures differed from the approach taken with heat flow because areas with very high standard error were assigned a confidence value of zero. The zone with the lowest confidence therefore had zero values for risk.

Groundwater temperature data (*e.g.,* Blackwell et al. 1992, Smith 2004, McLing et al. 2014, 2016) went through the same process used for heat flow data using EBK. This involved EBK interpolation to generate evidence and confidence layers.

The risk values for each element were calculated by multiplying the

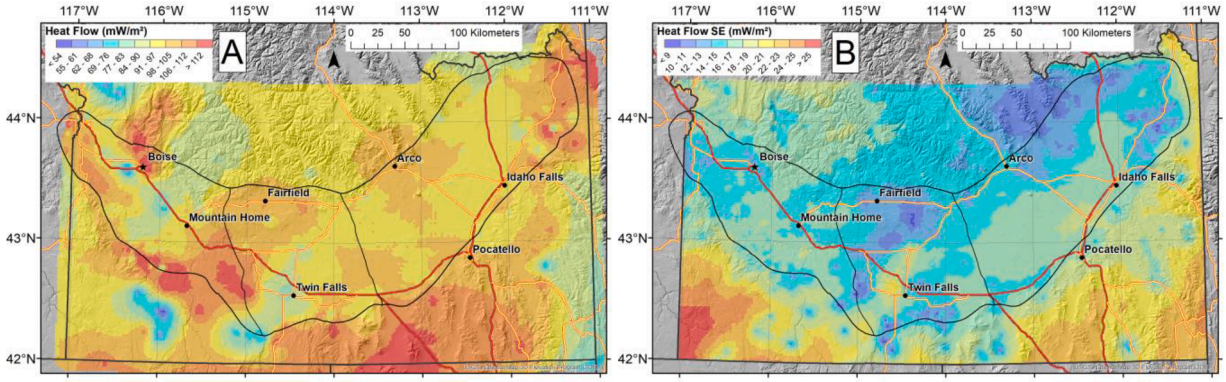

Fig. 6. (A) Estimated heat flow surface created using EBK from locations of measured heat flow. (B) Standard error of predicted heat flow surface created using EBK from locations of measured heat flow. Red and yellow lines represent roads. Hillshade from USGS 3D Elevation Program (U.S. Geological Survey, 2019).

scaled evidence and confidence values for layers that used confidence. Elements with no confidence had risk set equal to evidence. The CRS value for heat source was calculated by multiplying each risk element by its weight from the list of weights for heat source (Table 1), summing the products, and scaling the data (Fig. 7).

3.3. Seal

Two elements were examined in constructing the seal CRS map: lake sediments and aquifers. The lake sediment layer consisted of five polygons derived from regional geologic studies (Cluer and Cluer, 1986; Desborough et al., 1989; Anderson et al., 1997; Wood and Clemens, 2002). Each polygon was assigned a weight from a list as were areas with no lake sediments. The distribution of a regionally extensive shallow aquifer in the eastern SRP (Lindholm, 1996) was used to establish either the presence or absence of an aquifer deep enough to form an aquitard at its base to act as a seal; weights were established for both zones. Weights were generally high, ranging from 0.9 to 1.0 to effectively lower favorability by a small amount in areas with no seal or with a less confidence of an effective seal. The product of the weight values from lake sediments and aquifers became the CRS for seal. Seal CRS values are relatively high (~0.8–1.0) so that when multiplied by the weighted sum of the permeability and heat source CRS maps, overall favorability will remain higher in areas with better likelihood of an impermeable seal.

3.4. Composite common risk segment map

The CCRS map (Fig. 8) is the weighted (Table 1) sum of the permeability and heat source CRS maps multiplied by the Seal CRS map, then scaled from 0 - 1. All coefficients used in both phases were arrived at after a process of trial and error was employed to ensure coefficients appeared to produce reasonable results (*i.e.*, they do not overly-reflect elements that were thought to be less informative and/or less well-constrained) and show that known, deep, high-temperature wells have above average favorability.

Table 1
Weighting coefficients used in weighted sum calculations in Phase 1 and Phase 2. Weight coefficient values relate to the features in the data column in the order they appear.

Phase	Data	W	W	W	W	W	W
1	CCRS: Permeability, heat source	8	5				
1	CRS permeability: Mapped faults, magnetic, mid gravity, deep gravity	1	3	6	8		
1	CRS heat source: Vents, heat flow, helium, r-test, groundwater	30	55	5	5	5	
2	CCRS: Permeability, heat source	1	1				
2	CRS permeability: Mapped faults, magnetic, mid gravity, deep gravity	2	4	6	4		
2	CRS heat source: Vents, heat flow, helium, r-test, groundwater, sill	10	10	2	5	10	8

4. Phase 2 changes

4.1. Changes from Phase 1 to Phase 2

The second phase of the project focused on two subregions within the original Phase 1 study area: the Mountain Home and Camas Prairie study areas (Fig. 1). The study area for each region was examined at a higher resolution than the Phase 1 work, with Mountain Home using 500 m spacing and Camas Prairie using 100 m spacing. Coefficients used in Phase 2 weighted sum calculations were different than those used in Phase 1 (Table 1). Some elements were updated or added in Phase 2 work, with new field data added to the prior data compilation. Geophysical and other data (*e.g.*, Hill and Pakiser 1967, Nielson and Shervais 2014) document a presence of mafic sill in the mid-crust of the WSRP, similar to that observed in the ESRP. An outline of this inferred sill was added as an additional element in the heat source component. New sets of geophysical (gravity, magnetic) lineations were constructed for each study area, and new measures of confidence were applied for some data. Volcanic vent and helium isotope data were also updated with new locations.

A substantial change from Phase 1 involved using different length search radii when transforming data using density functions (Fig. 9). In both the Mountain Home and Camas Prairie regions, a 2.5 km radius was chosen for all evidence data except for helium data, which continued to use the 10 km buffer used in Phase 1 to reflect the wider area that could be representative of mantle influences.

4.2. Additional map types

The data releases associated with Phase 1 (DeAngelo et al., 2021a) and Phase 2 (DeAngelo et al., 2021b) contain evidence only and confidence only grids to compliment CCRS and CRS grids by separating out the effects of evidence and confidence (Fig. 10A–C). Grids showing the product (not a weighted sum) of all components, and the products of evidence only and confidence only are also included (Fig. 10 D–F). This is equivalent to the "veto equation" of Lautze et al. (2017a, 2017b). The product maps tend to highlight areas that are highly favorable for all components of the analysis, unlike the CCRS maps, which can still appear favorable if any individual component is not.

It can be seen in Fig. 10 that the CCRS map (Fig. 10A) qualitatively looks very similar to the evidence-only map (Fig. 10B), and that the effects from confidence on the CCRS map are mild in most places and moderate in very few areas. Product maps (Fig 10. D–F) and their equivalent modified weighted sum maps (Fig 10. A–C) show similar map patterns where relatively high and low favorability values exist, but the

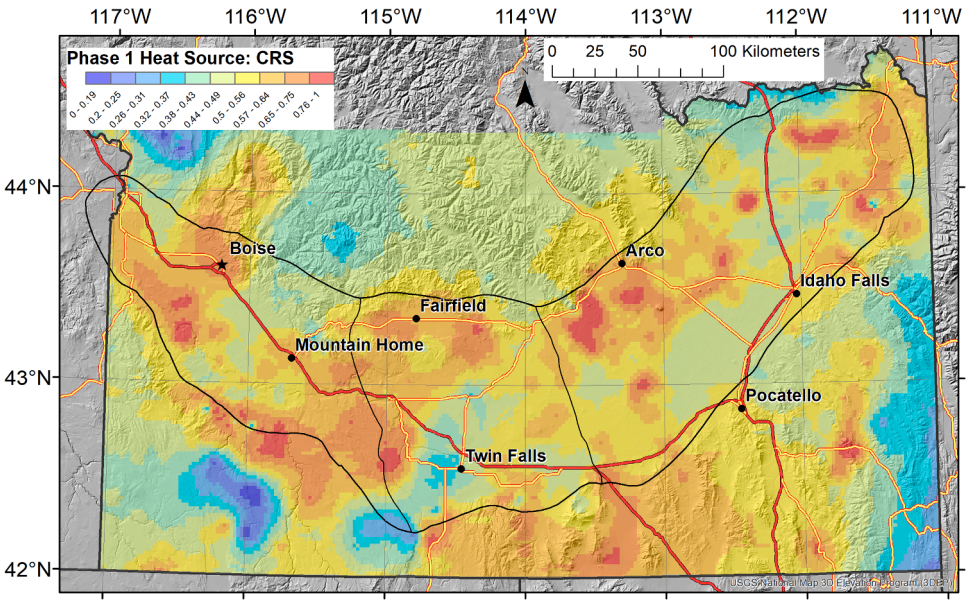

Fig. 7. Common risk segment (CRS) map for heat source. Warm colors indicate regions with high favorability. Red and yellow lines represent roads. Hillshade from USGS 3D Elevation Program (U.S. Geological Survey, 2019).

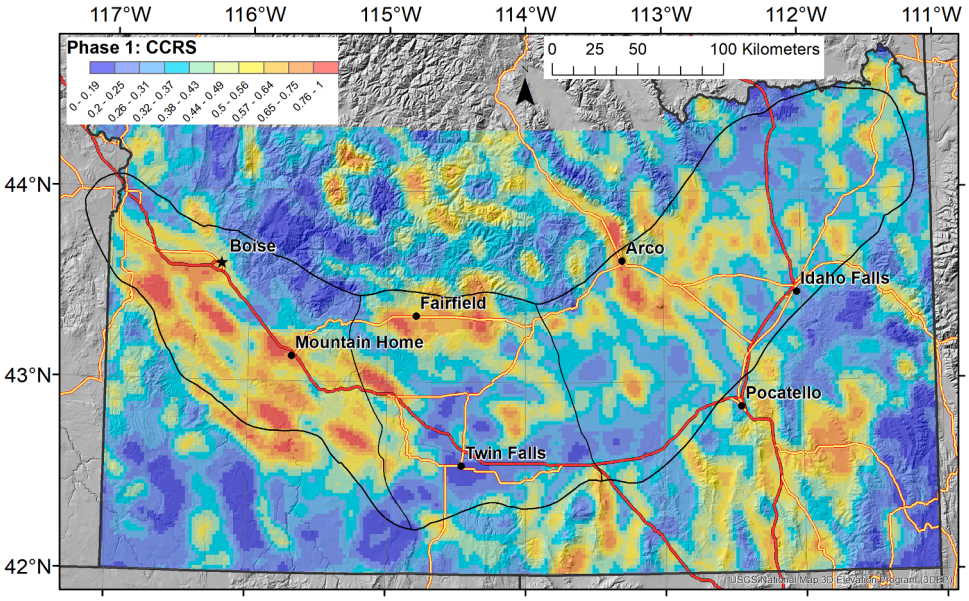

Fig. 8. Composite Common Risk Segment (CCRS) map. Warm colors indicate regions with high estimated geothermal favorability. Red and yellow lines represent roads. Hillshade from USGS 3D Elevation Program (U.S. Geological Survey, 2019).

product approach generated few moderate estimates of favorability, giving a starker contrast between areas of relatively high or low estimated favorability.

5. Discussion

The use of expert-chosen coefficients to define critical model parameters has both benefits and drawbacks. One possible benefit is using a weighted sum or product calculation makes it evident how each element contributes to favorability estimates in a simple model. Data-driven models sometimes produce results that appear counterintuitive, and it may be hard to know whether counterintuitive results are suffering from a lack of training data, non-ideal model design, or if the results indeed reflect something real and new. It seems that data-driven models and model parameters should always be preferable to expert-defined weightings in situations where there is high confidence that a data-driven approach will produce robust results. However, many settings for geothermal resource PFA do not have conditions that would allow for high confidence, robust data-driven approaches (*e.g.*, few data exist, etc.). Experts have limits in their ability to estimate ideal parameters but do possess insights that constrain a PFA-style assessment to physical reality by providing reasonable estimates. Expert decisions can help assure that coefficients used in weighted sums produce reasonable results, distance thresholds (density and distance functions) and weightings (by attributes like slip and dilation tendency for example) appear appropriate for the data and setting, and confidence associated with evidence data is properly identified and quantified. Therefore, this approach may be especially useful in settings with little training data or for comparisons with data-driven models that may benefit from having a simple, expert-constrained model to compare against.

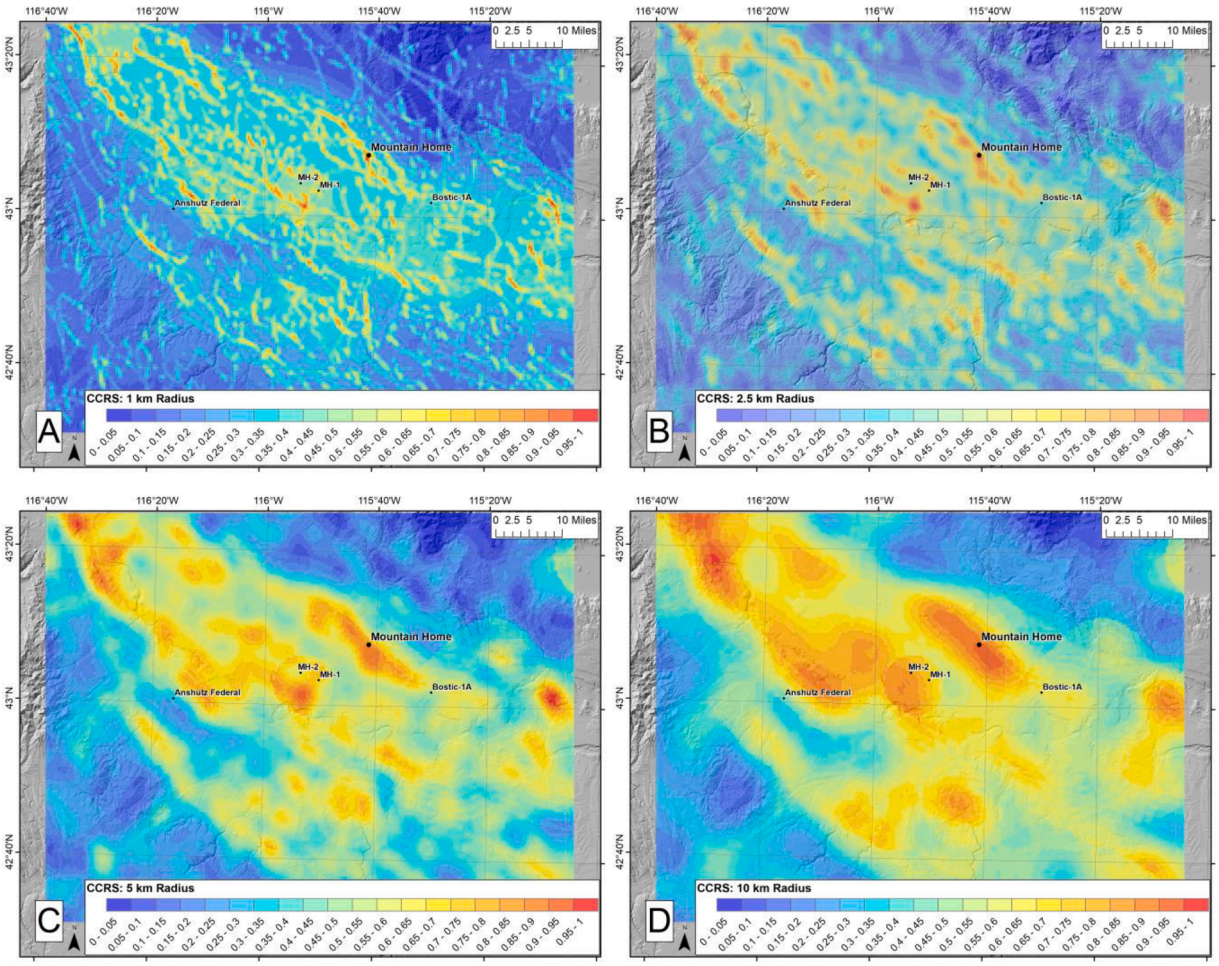

Fig. 9. Mountain Home example CCRS maps showing the effects of changing density function search radius length. All tools using a search radius, with the exception of helium data, used the following radius in the following plots: (A) 1 km, (B) 2.5 km (chosen for use in Phase 2), (C) 5 km, and (D) 10 km (used in Phase 1). Hillshade from USGS 3D Elevation Program (U.S. Geological Survey, 2019).

A potential weakness in this and any expert-driven approach is that many of the expert decisions (coefficients, distances, etc.) are poorly constrained by data, and any attempt to find reasonable results through expert opinion and trial and error could overly reflect the biases of experts. In Phase 1, trial and error guided modifications to coefficient weights in a process that led to certain elements being weighted more heavily within components, producing estimates that did not overly rely on any element in a way that appears to bias the results. For example, within the heat source component, data representing volcanic vents and background conductive heat flow were given far higher weights than data from the other elements (helium isotope data, multicomponent geothermometer water temperatures, groundwater temperatures) both due to higher confidence that they were modeled accurately, and they reflect processes that would be a better predictor of geothermal favorability. The exercise of trial and error was repeated in Phase 2 to settle upon coefficients and model parameters better suited to the subregions of Mountain Home and Camas Prairie.

Automated processing enabled values for weights, confidence, and other parameters to be modified in stand-alone tables, and the analysis could be repeated. This made it easier to test ideas, come up with a well-informed final product, and identify areas for further study. This approach could be applied to different settings, as demonstrated with Phase 2 work and in an example application to data from another PFA project in Washington (Forson et al., 2017; Shervais et al., 2021). Regions identified by Phase 1 for a more detailed Phase 2 analysis were examined through trial and error to identify a smaller cell size, shorter search distances for density functions, and different coefficients for weight and confidence values. Adapting this methodology to other geothermal settings can be done by adding and/or removing data layers (elements), modifying weights and other parameters, and defining a study area to suit the setting and available data.

This methodology is similar to those employed in other PFA projects (Lautze et al., 2017a; Forson et al., 2017; Faulds et al., 2018) in that it used expert-chosen weights to estimate geothermal favorability in a large region of the United States by either calculating a modified weighted sum (emphasizing moderate-strong presence of at least some critical components) or product (emphasizing strong presence of all components). In addition to the maps that show evidence, this methodology generated map products that include uncertainty in favorability estimates (CRS, CCRS, confidence-only maps) to account for data sparsity and modeling uncertainties. Our approach has been supported by slimhole drilling in one of our Phase 2 focus areas (Lachmar et al., 2023).

6. Conclusions

We have developed an approach to PFA for use in geothermal exploration that is based on previously published conceptual models *(e.g.,* Nielson and Shervais 2014, Nielson et al. 2015) and builds on methods used in earlier GIS and evidence-based approaches in geothermal exploration (*e.g.,* Coolbaugh et al. 2002, 2005, Noorollahi et al. 2008, Trumpy et al. 2015). Most of the processing is automated using a Python-based processing model, that enabled modifications to

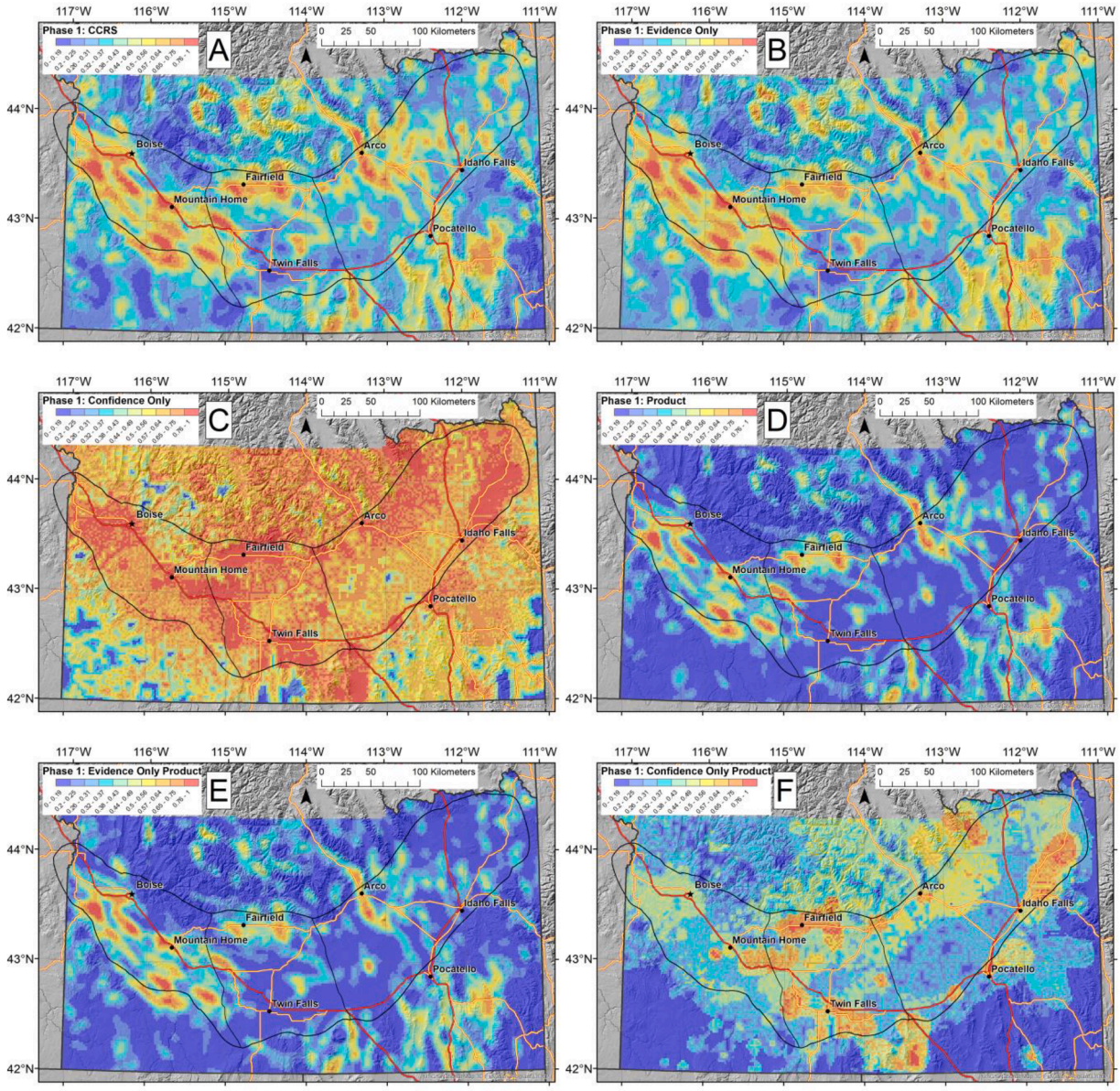

Fig. 10. Additional interpretive maps for comparison. (A) CCRS, (B) evidence-only, (C) confidence-only, (D) product, (E) evidence-only product, (F) confidence-only product. Red and yellow lines represent roads. Hillshade from USGS 3D Elevation Program (U.S. Geological Survey, 2019).

inputs, weights, and other important parameters informed by expert opinion and trial and error.

The three components we identified as being critical for the formation of a hydrothermal system in the SRP included a heat source (heat flow, vents, helium isotope ratios, calculated multicomponent equilibrium reservoir temperatures, measured groundwater temperatures, inferred sill), permeability (mapped faults and structures inferred from geophysics), and a seal (lake sediments and regional aquifers). Some elements had associated confidence data that accounted for data sparsity and modeling uncertainties. Expert-chosen coefficients were used to establish weighting relationships. Individual elements within heat and permeability components were combined using a weighted sum. These components were combined to create predictive surfaces, using either a weighted sum (CRS, CCRS maps) or by multiplying values (product map). Some models (CRS, CCRS maps) accounted for uncertainties in the underlying data layers, whereas others separated out the effects (evidence only and confidence maps).

Our approach helped to identify areas of high geothermal favorability in the western and central SRP during the first phase of study and was used to examine smaller study areas at a finer scale during the second phase of work, identifying more precise local drilling targets (Shervais et al., 2020). This approach, or any expert-driven analysis benefits from its simplicity but is fundamentally prone to inaccuracy and bias. By identifying favorable areas, the methodology presented here can reduce uncertainty in the initial stages of geothermal energy exploration and development in settings that could benefit from a simple, expert-constrained model. We caution, however, that no exploration strategy is risk free, and that in the end only a targeted program of drilling can confirm whether or not a viable resource is present (*e.g.,* Wilmarth et al. 2017, Lachmar et al., 2023).

Glossary

Common Risk Segment (CRS) map: Raster grid depicting a component's continuous range of values. The CRS maps for permeability and heat source are the weighted sum of risk layers from that component's elements. The CRS map for seal is the product of weight values.

Component: General geologic factor contributing to favorability,

comprised of permeability, heat source, and seal.

Composite Common Risk Segment (CCRS) map: Raster grid depicting the magnitude of the combined contributions of the study's CRS maps.

Confidence layer: Raster grid depicting an element's continuous range of uncertainty values.

Confidence-only map: The CRS-scale map depicts the weighted sum of the confidence layers within the permeability and heat source components; CCRS-scale map depicts the weighted sum of CRS-scale confidence-only maps of the permeability and heat source components.

Data-driven: An approach to weighting elements that relies on statistical relationships.

Data layer: ArcGIS shapefile in common projection used in making an evidence layer for an element, typically either point, line, or polygon data.

Element: Geologic factor being modeled in evidence, confidence and risk layers.

Empirical Bayesian Kriging (EBK): An iterative geostatistical interpolation method.

Evidence layer: Raster grid depicting an element's continuous range of values.

Evidence-only map: The CRS-scale map depicts the weighted sum of the evidence layers within the permeability and heat source components; CCRS-scale map depicts the weighted sum of CRS-scale evidence-only maps of the permeability and heat source components multiplied by CRS map for seal.

Heat source: One of the three components used in the study comprised of the following elements: Heat flow, volcanic vents, helium isotopic ratios, multicomponent equilibrium reservoir temperatures, and groundwater temperatures.

Interpolation: Process of estimating a raster surface of continuous values from point locations.

Kernel density function: Raster surface depicting spatial density of point locations with the density distributed from a maximum value at the center to a zero value at the limit of the full radius using a quadratic function. These locations can be given weighted values.

Knowledge-driven: An approach to weighting elements that relies on expert opinion.

Permeability: One of the three components used in the study comprised of the following elements: mapped faults, lineations interpreted from geophysics (mid-depth gravity and deep gravity), and magnetics.

Product map: A CCRS-scale map depicts the product of either evidence or confidence values from the three components, to create either an evidence product map or a confidence product map. This approach is intended to favor places that have high estimated favorability or confidence in all components, not just some.

Risk layer: Product of evidence and confidence layers; used in creating CRS map.

Seal: One of the three components used in the study comprised of the following elements: Lake sediments and aquifers.

Simple density function: Raster grid depicting spatial density of point locations. These locations can be given weighted values.

Submission declaration and verification

We certify that this work has not been published previously, that it is not under consideration for publication elsewhere, that its publication is approved by all authors and tacitly or explicitly by the responsible authorities where the work was carried out, and that, if accepted, it will not be published elsewhere in the same form, in English or in any other language, including electronically without the written consent of the copyright-holder.

CRediT authorship contribution statement

Jacob DeAngelo: Conceptualization, Methodology, Investigation, Resources, Formal analysis, Validation, Writing – review & editing. **John W. Shervais:** Project administration, Funding acquisition, Writing – original draft, Conceptualization, Methodology, Investigation, Resources, Formal analysis, Validation, Writing – review & editing. **Jonathan M. Glen:** Conceptualization, Methodology, Investigation, Resources, Formal analysis, Validation, Writing – review & editing, Supervision, Funding acquisition. **Dennis Nielson:** Conceptualization, Methodology, Investigation, Resources, Formal analysis, Validation, Writing – review & editing. **Sabodh Garg:** Conceptualization, Methodology, Investigation, Resources, Formal analysis, Validation, Writing – review & editing. **Patrick F. Dobson:** Conceptualization, Methodology, Investigation, Resources, Formal analysis, Validation, Writing – review & editing, Supervision, Funding acquisition. **Erika Gasperikova:** Conceptualization, Methodology, Investigation, Resources, Formal analysis, Validation, Writing – review & editing. **Eric Sonnenthal:** Conceptualization, Methodology, Investigation, Resources, Formal analysis, Validation, Writing – review & editing. **Lee M. Liberty:** Conceptualization, Methodology, Investigation, Resources, Formal analysis, Validation, Writing – review & editing. **Drew L. Siler:** Conceptualization, Methodology, Investigation, Resources, Formal analysis, Validation, Writing – review & editing. **James P. Evans:** Conceptualization, Methodology, Investigation, Resources, Formal analysis, Validation, Writing – review & editing.

Declaration of Competing Interest

The authors declare that they have no known competing financial interests or personal relationships that could have appeared to influence the work reported in this paper.

Data availability

10.5066/P95EULTI; 10.5066/P9Y8MEZY.

Acknowledgments

This work was supported by the U.S. Geological Survey Energy Resources Program, and by the U.S. Department of Energy Award EE-0006733. This work was also supported with funding by the Assistant Secretary for Energy Efficiency and Renewable Energy, Geothermal Technologies Office, of the U.S. Department under the U.S. Department of Energy Contract No. DE-AC02-05CH11231 with Lawrence Berkeley National Laboratory. Any use of trade, firm, or product names is for descriptive purposes only and does not imply endorsement by the U.S. Government.

References

Anderson, SR, Liszewski, MJ, and Cecil, LD, 1997, Geologic ages and accumulation rates of basalt-flow groups and sedimentary interbeds at the Idaho National Engineering Laboratory, Idaho. *USGS Water Resources Investigation Report* 97-4010, 39 pp.

Bankey, V., Cuevas, A., Daniels, D.L., Finn, C.A., Hernandez, I., Hill, P.L., Kucks, R., Miles, W., Pilkington, M., Roberts, C., Roest, W., 2002. Magnetic anomaly map of North America. US Geological Survey.

Bayes, T., 1764. An essay toward solving a problem in the doctrine of chances. Philos. Trans. R. Soc. Lond. 53, 370–418.

Blackwell, D.D., 1989. Regional implications of heat flow of the Snake River Plain, Northwestern United States. Tectonophysics 164, 323–343.

Blackwell, D.D. and M. Richards, 2004, Geothermal map of North America. American Association of Petroleum Geologists, Tulsa, Oklahoma, 1 sheet, scale 1:6,500,000.

Blackwell, D.D., Kelley, S., Steele, J.L., 1992. Heat flow modeling of the Snake River Plain, Idaho: D.O.E. contractor report no EGG-NPR-10790 109.

Bonham-Carter, G.F., 1994. Geographic Information Systems for Geoscientists: Modeling with GIS. Pergamon Press, Oxford, p. 269.

Cannon, C., Wood, T., Neupane, G., McLing, T., Mattson, E., Dobson, P., Conrad, M., 2014. Geochemistry sampling for traditional and multicomponent equilibrium

geothermometry in southeast Idaho. Geothermal Resources Council Transactions 38, 425–431.
Cluer, J.K., Cluer, B.L., 1986. The late Cenozoic Camas Prairie Rift, south-central Idaho. Rocky Mountain Geology 24, 91–101.
Coolbaugh, M.F., Taranik, J.V., Raines, G.L., Shevenell, L.A., Sawatzky, D.L., Minor, T.B., Bedell, R., 2002. A geothermal GIS for Nevada: defining regional controls and favorable exploration terrains for extensional geothermal systems. Geothermal Resources Council Transactions 26, 485–490.
Coolbaugh, M., Zehner, R., Kreemer, C., Blackwell, D., Oppliger, G., Sawatzky, D., Blewitt, G., Pancha, A., Richards, M., Helm-Clark, C., Shevenell, L., Raines, G., Johnson, G., Minor, T., Boyd, T., 2005, Geothermal potential map of the Great Basin, western United States: Nevada. Bureau of Mines and Geology Map (151).
DeAngelo, J., Shervais, J.W., Glen, J.M., Dobson, P.F., Liberty, L.M., Siler, D.L., Neupane, G., Newell, D.L., Evans, J.P., Gasperikova, E., Peacock, J.R., Sonnenthal, E., Nielson, D.L., Garg, S.K., Schermerhorn, W.D., and Earney, T.E., 2021a, Snake River Plain Play Fairway Analysis Phase 1 favorability model (DE EE0006733): U.S. Geological Survey data release, 10.5066/P95EULTI.
DeAngelo, J., Shervais, J.W., Glen, J.M., Dobson, P.F., Liberty, L.M., Siler, D.L., Neupane, G., Newell, D.L., Evans, J.P., Gasperikova, E., Peacock, J.R., Sonnenthal, E., Nielson, D.L., Garg, S.K., Schermerhorn, W.D., and Earney, T.E., 2021b, Snake River Plain Play Fairway Analysis Phase 2 favorability model (DE EE0006733): U.S. Geological Survey data release, doi:10.5066/P9Y8MEZY.
Desborough, G.A., Raymond, W.H. Marvin, R.F. and Kellogg, K.S., 1989, Pleistocene sediments and basalts along the Snake River in the area between Blackfoot and Eagle Rock, southeastern Snake River Plain, southeastern Idaho. U.S. Geological Survey Open-File Report 89-436, 18 pp.
Dobson, P.F., Kennedy, B.M., Conrad, M.E., McLing, T., Mattson, E., Wood, T., Cannon, C., Spackman, R., van Soest, M., Robertson, M., 2015. He isotopic evidence for undiscovered geothermal systems in the Snake River Plain. In: Proceedings of the 40th Workshop on Geothermal Reservoir Engineering. Stanford University, Stanford, CA, 7 p.
Drenth, B.J., Grauch, V.J.S., 2019. Finding the gaps in America's magnetic maps. EOS Scie. News 100. https://doi.org/10.1029/2019EO120449.
Esri, 2023. ArcPro desktop: release 3.0.2. Environmental Systems Research Institute, Redlands, CA.
Faulds, J.E., Hinz, N.H., 2015. Favorable tectonic and structural settings of geothermal systems in the Great Basin region, Western USA: proxies for discovering blind geothermal systems. In: Proceedings of the World Geothermal Congress. Melbourne, Australia, 19-25, p. 6. April 2015.
Faulds, J.E., Craig, J.W., Coolbaugh, M.F., Hinz, N.H., Glen, J.M., Deoreo, S., 2018, Searching for blind geothermal systems utilizing play fairway analysis, western Nevada, Geothermal Resources Council Bulletin, 47, p. 34–42.
Ferrill, D.A., Winterle, J., Wittmeyer, G., Sims, D., Colton, S., Armstrong, A., Morris, A.P., 1999. Stressed rock strains groundwater At Yucca Mountain, 9. GSA Today, Nevada, pp. 1–8.
Forson, C., Steely, A., Cladouhos, T., Swyer, M., Davatzes, N., Anderson, M., Ritzinger, B., Glen, J., Peacock, J., Schermerhorn, W., Burns, E., Stelling, P., 2017, Washington geothermal play fairway analysis technical report. Retrieved from: http://gdr.openei.org/submissions/994.
Hildenbrand, T.G., Briesacher, A., Flanagan, G., Hinze, W.J., Hittelman, A.M., Keller, G. R., Kucks, R.P., Plouff, D., Roest, W., Seeley, J., Smith, D.A., and Webring, M., 2002, Rationale and operational plan to upgrade the U.S. Gravity Database: U.S. Geological Survey Open-File Report 02-463, 12p.
Hill, D.P., Pakiser, L.C., 1967. Crustal structure between the Nevada test site and Boise Idaho from seismic refraction measurements. Steinhart and Smith (eds). In: The Earth Beneath the Continents, 10. American Geophysical Union Monograph, pp. 391–419.
Ito, G., Frazer, N., Lautze, N.C., Thomas, D., Hinz, N., Waller, D., Whittier, R., Wallin, E., 2017. Play fairway analysis of geothermal resources across the State of Hawai'i: 2. Resource probability mapping. Geothermics 70, 393–405. https://doi.org/10.1016/j.geothermics.2016.11.004.
Krivoruchko, K., Gribov, A., 2020. Empirical Bayesian kriging implementation and usage. Sci. Total Environ. 722 https://doi.org/10.1016/j.scitotenv.2020.137290. VolumeISSN 0048-9697.
Lachmar, T.E., Freeman, T.G., Sant, C.J., Walker, J.R., Batir, J.F., Shervais, J.W., Evans, J.P., Nielson, D.L., Blackwell, D.D., 2017. Effect of an 860-m thick, cold, freshwater aquifer on geothermal potential along the axis of the eastern Snake River Plain, Idaho. Geotherm. Energy 5, 28. https://doi.org/10.1186/s40517-017-0086-8.
Lachmar, T.E., Freeman, T.G., Kessler, J.A., Batir, J.F., Evans, J.P., Nielson, D.L., Shervais, J.W., Chen, X., Schmitt, D.R., Blackwell, D.D., 2019. Evaluation of the geothermal potential of the western Snake River Plain based on a deep corehole on the Mountain Home AFB near Mountain Home, Idaho. Geotherm. Energy 7, 26. https://doi.org/10.1186/s40517-019-0142-7.
Lachmar, T.E., Neupane, G., Garg, S.K., Dobson, P.F., Smith, C.J., Newell, D.L., Shervais, J.W., Evans, J.P., Mink, L.L., 2023. Validation of Play Fairway Analysis of the geothermal potential of Camas Prairie, south-central Idaho, by an exploration well. Geotherm. Energy 11 (1), 21. https://doi.org/10.1186/s40517-023-00264-4.
Lautze, N.C., Thomas, D., Hinz, N., Ito, G., Frazer, N., Waller, D., 2017a. Play fairway analysis of geothermal resources across the State of Hawai'i: 1. Geological, geophysical, and geochemical datasets. Geothermics 70, 376–392. https://doi.org/10.1016/j.geothermics.2017.02.001.
Lautze, N.C., Thomas, D., Waller, D., Hinz, N., Frazer, N., Ito, G., 2017b. Play fairway analysis of geothermal resources across the State of Hawai'i: 3. Use of development viability criterion to prioritize future exploration activities. Geothermics 70, 406–413. https://doi.org/10.1016/j.geothermics.2017.07.005.
Lindholm, G.F., 1996, Summary of the Snake River regional aquifer-system analysis in Idaho and eastern Oregon: U.S. Geological Survey Professional Paper 1408-A. doi:10.3133/pp1408A.
Ludington, S., Moring, B.C., Miller, R.J., Evans, J.G., Stone, P.S., Bookstrom, A.A., Nutt, C.J., Bedford, D.R., Haxel, G.A., Hopkins, M.J., Flynn, K.S., 2005. Preliminary integrated geologic map databases for the United States - Western states: California, Nevada, Arizona, Washington, Oregon, Idaho, and Utah. USGS. https://doi.org/10.3133/ofr20051305.
Machette, M.N., Haller, K.M., Dart, R.L., Rhea, S.B., 2003, Quaternary fault and fold database of the United States: U.S. Geological Survey Open-File Report 03-417.
McCafferty, A.E., Kucks, R.P., Hill, P.L., Racey, S.D., 1999, Aeromagnetic map for the State of Idaho, U.S. Geological Survey Open-File Report 99-371. doi:10.3133/ofr99371.
McLing, T., McCurry, M., Cannon, C., Neupane, G., Wood, T., Podgorney, R., Welhan, J., Mines, G., Mattson, E., Palmer, G., Smith, R., 2014. David Blackwell's forty years in the Idaho Desert, the foundation for 21st Century geothermal research. Geothermal Resources Council Transactions 38, 143–153.
McLing, T.L., Smith, R.P., Smith, R.W., Blackwell, D.D., Roback, R.C., Sondrup, A.J., 2016. Wellbore and groundwater temperature distribution eastern Snake River Plain, Idaho: implications for groundwater flow and geothermal potential. J. Volcanol. Geotherm. Res. 320, 144–155.
Morris, A., David, A.F., Henderson, B., 1996. Slip-tendency analysis and fault reactivation. Geology 24, 275–278.
Neupane, G., Mattson, E.D., McLing, T.L., Palmer, C.D., Smith, R.W., Wood, T.R., 2014. Deep geothermal reservoir temperatures in the Eastern Snake River Plain, Idaho using multicomponent geothermometry. In: Proceedings of the Thirty-Eighth Workshop on Geothermal Reservoir Engineering. Stanford, California. Stanford University. February 24-26, 2014 SGP-TR-202.
Nielson, D.L., Shervais, J.W., 2014. Conceptual model of Snake River Plain geothermal systems. In: Proceedings of the Thirty-Ninth Workshop Geothermal Reservoir Engineering, 2014. Stanford University, pp. 1010–1016.
Nielson, D.L., Shervais, J.W., Liberty, L., Garg, S.K., Glen, J., Visser, C., Dobson, P., Gasperikova, E., Sonnenthal, E., 2015. Geothermal Play Fairway Analysis of the Snake River Plain, Idaho. In: Proceedings of the Fortieth Workshop on Geothermal Reservoir Engineering. Stanford, California. Stanford University. January 26-28, 2015 SGP-TR-204.
Noorollahi, Y., Itoi, R., Fujii, H., Tanaka, T., 2008. GIS integration model for geothermal exploration and well siting. Geothermics 37, 107–131. https://doi.org/10.1016/j.geothermics.2007.12.001.
Shervais, J.W., Evans, J.P., Schmitt, D., Christiansen, E.H., Prokopenko, A.A., 2014. Drilling into the track of the yellowstone hot spot. EOS, Trans. Am. Geophys. Union. 95 (10), 85–86. https://doi.org/10.1002/2014EO100001.
Shervais, J.W., DeAngelo, J., Glen, J.M., Nielson, D.L., Garg, S., Dobson, P., Gasperikova, E., Sonnenthal, E., Liberty, L.M., Newell, D.L., Siler, D., Evans, J.P., 2024. Geothermal play fairway analysis, part 1: Example from the Snake River Plain, Idaho. Geothermics 117, 102865.
Shervais, J.W., Glen, J.M., Liberty, L.M., Dobson, P., Gasperikova, E., Sonnenthal, E., Visser, C., Nielson, D., Garg, S., Evans, J.P., Siler, D., DeAngelo, J., Athens, N., Burns, E., 2015. Snake River Plain Play Fairway Analysis - Phase 1 report. Geothermal Resources Council Transactions 39, 761–769.
Shervais, J.W., Evans, J.P., Glen, J.M., DeAngelo, J., Dobson, P., Gasperikova, E., Sonnenthal, E., Siler, D., Liberty, L.M., Visser, C., Nielson, D.L., Garg, S., Athens, N., Burns, E., 2016, Snake River plain play fairway analysis: phase 1 final report, Report to Department of Energy Geothermal Technology Office, Project number DE-EE 0006733. Retrieved from: https://gdr.openei.org/submissions/1231.
Shervais, J.W., Evans, J.P., Glen, J.M., DeAngelo, J., Dobson, P., Gasperikova, E., Sonnenthal, E., Siler, D., Liberty, L.M., Visser, C., Nielson, D.L., Garg, S., Athens, N., Burns, E., 2020, Snake river plain play fairway analysis: phase 2 report and phase 3 proposal, Report to Department of Energy Geothermal Technology Office, Project number DE-EE 0006733. Retrieved from http://gdr.openei.org/submissions/1232.
Shervais, J.W., Evans, J.P., Glen, J.M., DeAngelo, J., Dobson, P., Gasperikova, E., Sonnenthal, E., Siler, D., Liberty, L.M., Visser, C., Nielson, D.L., Garg, S., Athens, N., Burns, E., 2021, Play fairway analysis of the Snake River Plain, Idaho: final Report, Report to Department of Energy Geothermal Technology Office, Project number DE-EE 0006733. Retrieved from http://gdr.openei.org/submissions/1316.
Siler, D.L., Faulds, J.E., Mayhew, B., McNamara, D.D., 2016. Analysis of the favorability for geothermal fluid flow in 3D: astor Pass geothermal prospect, Great Basin, northwestern Nevada, USA. Geothermics 60, 1–12.
Smith, R.P., 2004. Geologic setting of the Snake River Plain Aquifer and vadose zone. Vadose Zone J. 3, 47–58.
Trumpy, E., Donato, A., Gianelli, G., Gola, G., Minissale, A., Montanari, D., Santilano, A., Manzella, A., 2015. Data integration and favourability maps for exploring geothermal systems in Sicily, southern Italy. Geothermics 56, 1–16. https://doi.org/10.1016/j.geothermics.2015.03.004.
U.S. Geological Survey, 2019. 3D Elevation Program 1-Meter Resolution Digital Elevation Model. https://www.usgs.gov/the-nationalmap-data-delivery.
Van Rossum, G., Drake Jr., F.L., 1995. Python reference manual. Centrum Wiskunde & Informatica, Amsterdam.
Wilmarth, M., Haizlip, J., Cumming, W., 2017. Tutuila, American Samoa: a case history of geothermal exploration on a Deep Sea Island. In: Proceedings of the 42nd Workshop on Geothermal Reservoir Engineering. Stanford, California. Stanford University. February 13-15, 2017 SGP-TR-212.

Williams, C.F., DeAngelo, J., 2008. Mapping geothermal potential in the Western United States. Geothermal Resources Council Transactions 32, 181–188.
Williams, C.F., DeAngelo, J., 2011. Evaluation of approaches and associated uncertainties in the estimation of temperatures in the upper crust of the western United States. Geothermal Resources Council Transactions 35, 1599–1605.
Wood, S.H., Clemens, D.M., 2002. Geologic and tectonic history of the western Snake River Plain, Idaho and Oregon. Bonnichsen B., White C., and McCurry M., eds Tectonic and Magmatic Evolution of the Snake River Plain Volcanic Province. Idaho Geological Survey Bulletin 30, Moscow, ID, United States, pp. 69–103.